九州大学学術情報リポジトリ
Kyushu University Institutional Repository

Modeling High Frequency 13.56 MHz Full Bridge Inverter Based on GaN MOSFET for EV Wireless Charging System

Meiyanto Eko Sulistyo
Department of Electrical Engineering, Universitas Sebelas Maret (UNS)

Gustav Lukman Adhi Pradhityo
Department of Electrical Engineering, Universitas Sebelas Maret (UNS)

Muharam, Aam
Research Center for Transportation Technology, National Research and Innovation Agency, Indonesia

Nugroho, Asep
Research Center for Smart Mechatronics, National Research and Innovation Agency, Indonesia

他

https://doi.org/10.5109/7151734

出版情報：Evergreen. 10 (3), pp.1847-1854, 2023-09. 九州大学グリーンテクノロジー研究教育センター
バージョン：
権利関係：Creative Commons Attribution-NonCommercial 4.0 International

KYUSHU UNIVERSITY

Modeling High Frequency 13.56 MHz Full Bridge Inverter Based on GaN MOSFET for EV Wireless Charging System

Meiyanto Eko Sulistyo[1,*], Gustav Lukman Adhi Pradhityo[1], Aam Muharam[2], Asep Nugroho[3], Amin[2], Sunarto Kaleg[2], Alexander Christhanto Budiman[2], Sudirja[2], Rina Ristiana[2], Reiji Hattori[4]

[1]Department of Electrical Engineering, Universitas Sebelas Maret (UNS), Indonesia
[2]Research Center for Transportation Technology, National Research and Innovation Agency, Indonesia
[3]Research Center for Smart Mechatronics, National Research and Innovation Agency, Indonesia
[4]Department of Applied Science for Electronics and Materials, Kyushu University, Japan

*Author to whom correspondence should be addressed:
E-mail: mekosulistyo@staff.uns.ac.id

(Received April 27, 2023; Revised June 20, 2023; accepted July 4, 2023).

Abstract: This paper presents a modelling of a high-frequency full bridge inverter for wireless power transmission (WPT) in Electric Vehicle (EV) charging applications. The inverter is designated at an operating frequency as high as 13.56 MHz in line with regulations for the industrial, scientific, and medical radio band (ISM band). Since the power is transferred wirelessly from the source to the EV, a coupling capacitive was used as a transmitter and receiver of the system. In this paper, the inverter model was simulated and analysed using LTSpice software. Different load changes and power are injected into the system. Furthermore, in order to obtain a robust system, the switching frequency of 13.56 MHz is used with some Dead Time (DT). The system already uses GaN MOSFETs for reliability and performance at high frequencies, in addition to LC impedance matching. The result is that by operating at a resonant frequency of 13.56 MHz with a resistive load of 50, it is obtained with a power of 2.3 kW that has been successfully transmitted with an efficiency of 89%.

Keywords: inverter; full-bridge; wireless power transfer; electric vehicle

1. Introduction

At this time, a lot of research is being done on wireless power transfer (WPT) because it can transfer energy without physical contact. Because it is considered more profitable from a security point of view, it is then used for various fields of application[1–5] including for charging cellphone batteries, biomedical implants, and charging electric vehicles (EV) capable of charging systems up to kilowatts. Research related to the charge and discharge battery phenomena[6,7], considering some heat management of battery pack[8], energy management for EV system[9], and microwave propagation[10] has been conducted.

Based on this application, resonance capable of working at megahertz (MHz) can be used for lower power and smaller system sizes[5]. For operating systems with high frequencies ranging from 6.78 MHz and 13.56 MHz, this will be used more for WPT systems which are more precise and lighter as they are able to transfer energy over longer distances. If using a kHz frequency system there will be losses such as the number of components that result in a larger system design. But when making a WPT system with MHz resonance there will be losses in the form of component parasitic elements and considering each component.

The high-frequency inverter is suitable for powering multi-MHz WPT systems. Class-E and Class-D amplifier topologies that work at MHz frequencies have been discussed in the literature[11–15]. In Class-D amplifier design, the input voltage is square which does not consider the off time, further very important to high frequencies applications.

This paper will describe the design of a high-frequency inverter that will be applied to an EV charging system using LTSpice software. Various variations were carried out to identify the output power efficiency produced by the inverter, ranging from variations in input voltage to loads ranging from 10-100. A designated full bridge inverter using GaN MOSFET, with 13.56 MHz high-frequency operation and some additional Dead Time applied, resulted in over 2.3 kW power with 89% of power

efficiency.

2. Wireless power transfer (WPT)

Several WPT technologies use electric, magnetic, and electromagnetic fields as a way of transmitting electrical energy without using cables. WPT is useful for powering electrical devices where the cable used is inconvenient, dangerous, or impossible. The techniques fall into two categories: non-radiative and radiative. In near-field or non-radiative engineering, power is transferred by a magnetic field using inductive coupling between coils of wire, or an electric field using capacitive coupling between metal electrodes. Table 1 shows the comparison of the three-coupling type of WPT.

Table 1. Comparison of wireless power transfer coupling[16].

	coupling type		
	Inductive	**Magnetic Resonant**	**Capacitive**
Frequency	Low	High	High
Distance	Short	Medium	Medium
Method	Coil	Resonator	Capacitor
Field	Magnetic	Resonance	Electric
Efficiency	High	High	High

In general, the WPT system is divided into three parts, namely the DC-AC inverter (source), the coupling, and the AC-DC rectifier (load)[17]. In the WPT magnetic field coupling system, two coils are used in the coupling section, which is often represented as a transformer with a low coupling coefficient in electric circuit models. In the transmitter, it is necessary to generate an AC flowing through the primary coil, which is achieved by a DC-AC inverter. At the receiving end, the received AC needs to be converted into DC voltage, which is done by an AC-DC rectifier. It is important to reduce power losses in each section to achieve high power delivery efficiency in a WPT system.

Inductive Power Transfer (IPT) has been widely implemented for electric vehicle (EVs) charging and small electronic device battery charging, on the other hand, IPT has weaknesses because it utilizes electromagnetic induction such as EMI, cannot penetrate metal media, and eddy currents[18].

The concept of capacitive power transfer (CPT) is the same as IPT, but the difference is that the intermediary medium for power delivery uses a capacitive plate by generating an electric field that arises from the plate. Since wireless power transmission works by resonant frequency, the International Telecommunications Union defines ISM[19].

CPT has rules for its frequency set by the ISM bands which are 6.78 MHz, 13.56 MHz, and so on [20]. Furthermore, CPT technology was developed as an alternative to IPT technology due to the following factors, namely low eddy current losses, low EMI, fewer components required, and the ability to transfer electric current. through metal objects. CPT technology is used not only in WPT for battery charging but also in data and signals transmission[21–24].

As can be seen from Fig. 1, this system has 2 cores consisting of a sending side and a receiving side. For the sending side, the harmonics will be matched first by the LC filter, then it will go through the rectifier to convert power from AC to DC, and finally it will be converted back to DC-AC by an inverter but with a high frequency.

When the two opposite sides of the plate are definite and active, they will be able to produce an alternating electric field so that the transmission of power from the sending side to the receiving side can be carried out[25]. For the receiving side, you must use a rectifier again because the power obtained is still in the form of AC so that it becomes DC so that the electric power can be received by the load.

3. RF power characteristic

3.1 High-frequency switching device

Inverter is a power electronics circuit that functions to convert DC voltage to AC. Today, inverters have many

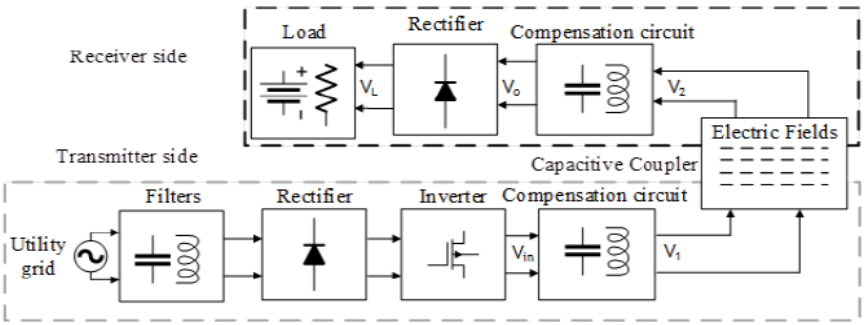

Fig. 1: Structure of capacitive power transfer[16]

topologies but the ones used for CPT are capable of pure sinusoidal output. In addition, inverters can be categorized based on their phases, which start from one phase to three phases, while this research aims to obtain a fairly high resonant frequency, namely 13.56 MHz.

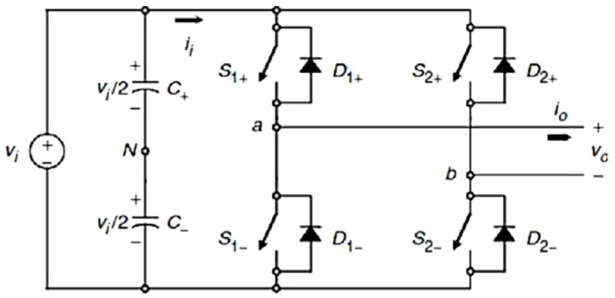

Fig. 2: Full bridge inverter circuit model[16)]

Fig. 2 illustrates the circuit model of the full bridge inverter. The switch used for the inverter must have a fast response to change from the OFF state to the ON or vice versa. Therefore, a MOSFET (Metal Oxide Semiconductor Field Effect Transistor) type switching device is used. An inverter is said to be ideal if the output voltage waveform is purely sinusoidal. Power semiconductors with a wide bandgap (WBG) are being used in an increasing number of applications. Because Gallium Nitride (GaN) devices are lateral and Silicon Carbide (SiC) devices are vertical, commercially available GaN devices have lower voltage ratings than SiC devices. However, because of their size and structure, GaN devices have lower device capacitance (C_{oss}, C_{iss}), making them easier to drive at higher frequencies. These features divide the WBG market into two parts: SiC is utilized in higher voltage and lower frequency applications, whereas GaN is employed in lower voltage and higher frequency applications[26)].

3.2 Impedance matching

Impedance matching can be defined as designing or matching the value of the power source's input impedance with the electrical load's output impedance so that the power transfer to the load can be maximized. Impedance matching can be interpreted to match a 50 Ω impedance load with an LC filter so that the maximum power transfer is at a frequency of 13.56 MHz.

When the inverter output with a frequency of 13.56 MHz is in the form of a square signal, it is necessary to have an LC filter to filter and convert the box signal to sinusoidal so that it can be used and does not damage the load device. The LC filter is used to pass or only work at a frequency of 13.56 MHz by adjusting the load impedance of 50 Ω so that the power distribution can be maximized.

According to the maximum power transfer theorem, when the load resistance is equal to the source resistance and the load reactance is equal to the negative of the source reactance, the maximum power is transferred from the source and load. This means that maximum power can be transferred if the load impedance is equal to the complex conjugate of the source impedance.

In the case of DC circuits, frequency is not considered. Therefore, the condition is met if the load resistance is equal to the source resistance. In the case of an AC circuit, the reactance is frequency-dependent. Therefore, if the impedance is suitable for one frequency it may not match if the frequency is changed. Calculation of the LC filter design with a load of 50 Ω and a working frequency of 13.56 MHz is as follows, inductor value calculation:

$$L = \frac{\sqrt{2} \times R_l}{\omega} \quad (1)$$

$$R_l = \frac{(R)}{2} \quad (2)$$

the calculation for the capacitor value C can be obtained by:

$$C = \frac{1}{(\omega \times R_l \times \sqrt{2})} \quad (3)$$

where $\omega = 2\pi f$.

3.3 Dead time

Dead time is a PWM technique that is carried out on a full bridge inverter circuit to give a gap time to the GaN MOSFET so that it doesn't happen simultaneously which can cause a short circuit and damage the GaN MOSFET. The lag time is given when the high side GaN MOSFET has a high value and then wants to go low there while the low side GaN MOSFET wants to be high there is a time difference so that it does not turn ON and OFF at the same time.

Look for the dead time value of the 10% PWM difference for T_{on} and T_{off} conditions with the GaN MOSFET reference being at the high side. The value of T_{on_high} can be calculated as:

$$T_{on_high} = \frac{T_{period}}{2} \quad (4)$$

$$T_{period} = \frac{1}{f_{resonant}} \quad (5)$$

where the value of T_{on_low} can be obtained as:

$$T_{on_low} = 60\% \times T_{period,} \quad (6)$$

While delay time between the high side and low side period can be defined as:

$$T_{death\ time} = \frac{(10\% \times T_{period})}{2} \quad (7)$$

Then the low side time delay can be obtained as:

$$T_{delay_low} = T_{delay_high} - T_{death\ time}. \quad (8)$$

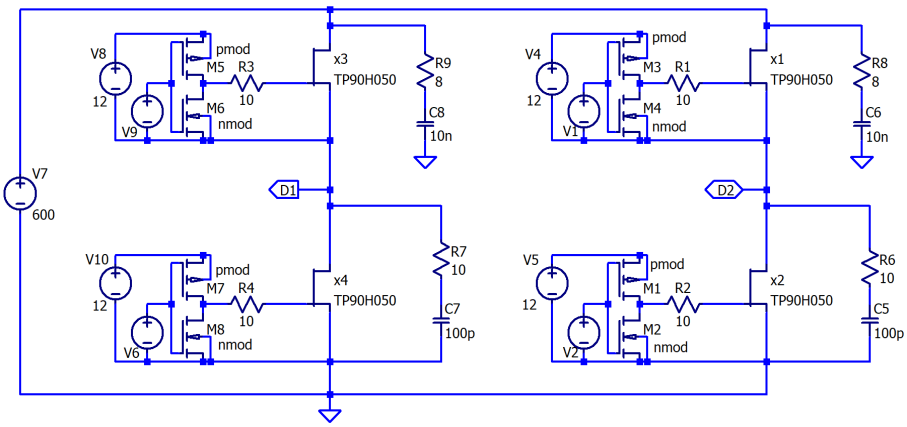

Fig. 3: Full bridge inverter circuit simulation model

4. Simulation and design results

Prior to the direct testing of components, simulations were carried out using LTSpice software. Simulations are carried out to determine the output of the full bridge inverter signal with a frequency of 13.56 MHz as well as to calculate the dead time so that there is no short circuit when the GaN MOSFET enters the transition from OFF to ON condition and vice versa. The circuit model of the full bridge inverter for the simulation process is shown in Fig. 3. It can be seen a gate driver MOSFET appears for each switching device that is constructed with TP90H050 GaN MOSFET. By using the equation (1) to (3), the value of LC filter components then can be acquired.

The concept used for the GaN MOSFET driver in this simulation uses the totem pole MOSFET driver. The driver consists of two MOSFETs that function as a switch for OFF and ON conditioning, therefore, controlling switching with high frequency to achieve high speed and accuracy. For other totem pole drivers, it can also use 2 bi-junction transistors (BJTs). However, driving high-frequency GaN MOSFET requires high accuracy and speed. This is a weakness of 2 BJTs, therefore it is replaced by 2 MOSFET.

The working operation of the totem pole driver is described as:

- When PWM is low or "0" it will be read by the high MOSFET so that the VDD voltage enters the *pmod* and current will flow through to open the gate driver which makes VGs > Vth, therefore the GaN MOSFET is ON.

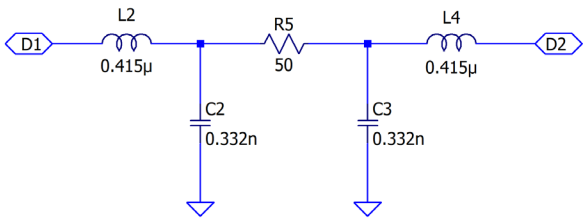

Fig. 4: Designated LC filter

- When the PWM value is high or "1" it will be read by the low MOSFET so that the voltage and current will be drawn into the *nmod* MOSFET and then discharged through the ground therefore no voltage will enter the MOSFET gate so the GaN MOSFET is in the OFF condition.

Fig. 4 shows the designated LC filter as well as results by the formula. The inductor value is 0.415 µH and the capacitor value is 0.332 nF which is used as an LC filter to limit the working frequency to 13.56 MHz. Furthermore, the calculation results are entered into the LTSpice simulation to find out and see the output signal from the full bridge inverter.

In order to find the value for T_{on_high}, by using Equations (4) and (5), here is the frequency value for the input PWM signal in the gate driver to control the GaN MOSFET can be obtained as:

$$T_{period} = \frac{1}{13.56\ MHz} = 0.1475\ \mu s$$

$$T_{on_high} = \frac{0.1475\ \mu s}{2} = 0.07374 \mu s$$

then it is entered into the MOSFET driver parameter as a timer for the GaN MOSFET in OFF and ON conditions. For the ON time value is equal to the delay time because it is a reference for setting the low-side driver.

The time ON value for the low side driver can be obtained by using Equation (6) followed by Equation (7) for the delay time with the high side time value as a reference. The value acquired as:

$$T_{on_low} = 60\% \times 0.1475\ \mu s = 0.0885\ \mu s$$

$$T_{death\ time} = \frac{(10\% \times 0.1475\ \mu s)}{2} = 0.007375\ \mu s$$

To find the delay time of the low side driver, it is obtained by reducing the value of the high side delay time

Table 2. Driver setting parameters.

Parameter	Setting Value		
	High side	Low side	Unit
$V_{initial}$	12	0	V
V_{on}	0	12	V
T_{delay}	0.07374	0.066365	µs
T_{rise}	2		ns
T_{fall}	1		ns
T_{on}	0.07374	0.0885	µs
T_{period}	0.14749		µs

and the delay time with 10% PWM. By using equation (8), the delay time value of the low side driver can be obtained as:

$$T_{delay_low} = 0.07374\ \mu s - 0.007375\ \mu s$$
$$= 0.066365\ \mu s$$

Table 2 shows the setting value for the high-side and low-side GaN MOSFET drivers parameters based on the calculation. Thus, the switching diagram of gate driver MOSFET shown on Fig. 5. It can be seen in Fig.5.(a), the switching condition of totem pole MOSFET gate driver. The switching state VM5 is vice versa with VM6 as same as VM7 and VM8 diagram state.

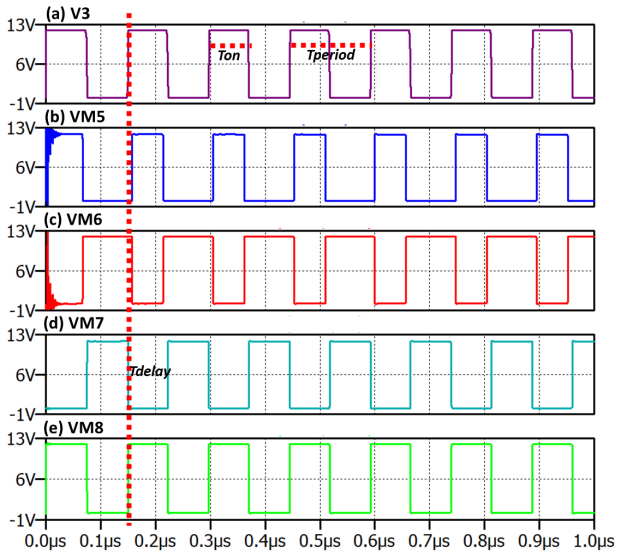

Fig. 5: Switching diagram of gate driver MOSFET

The output voltage signal from the inverter can be measured at D1 and D2 points. It can be seen from Fig. 6, that the voltage signal at D1 (marked with a blue line) has an amplitude of 600 V as well as the voltage signal at D2 (marked with a red line), but with the opposite operation when it's ON and OFF. The signal confirmations the operation of both high side MOSFET and low side MOSFET in the full bridge inverter that is in complimentary generated.

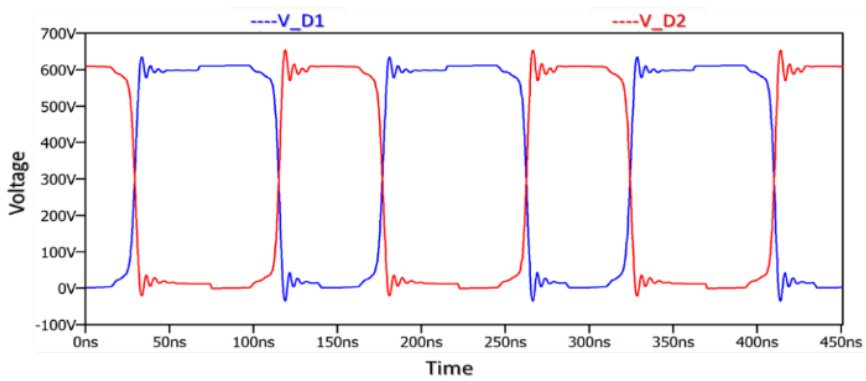

Fig. 6: MOSFET output voltage waveform D1 and D2

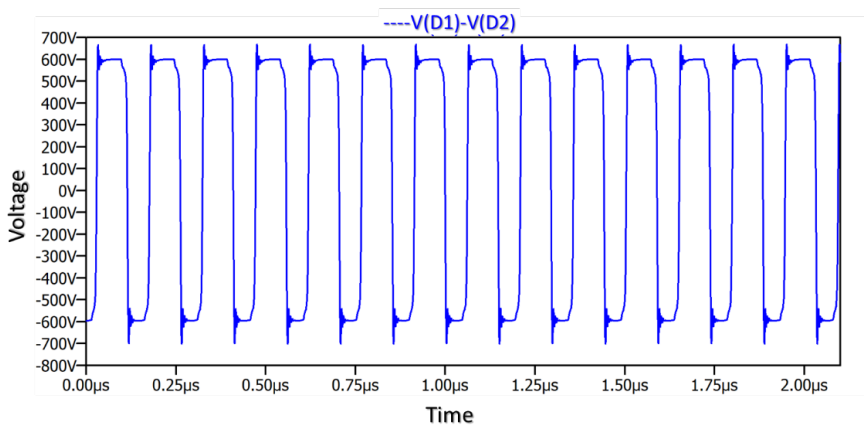

Fig. 7: MOSFET output voltage waveform D1-D2

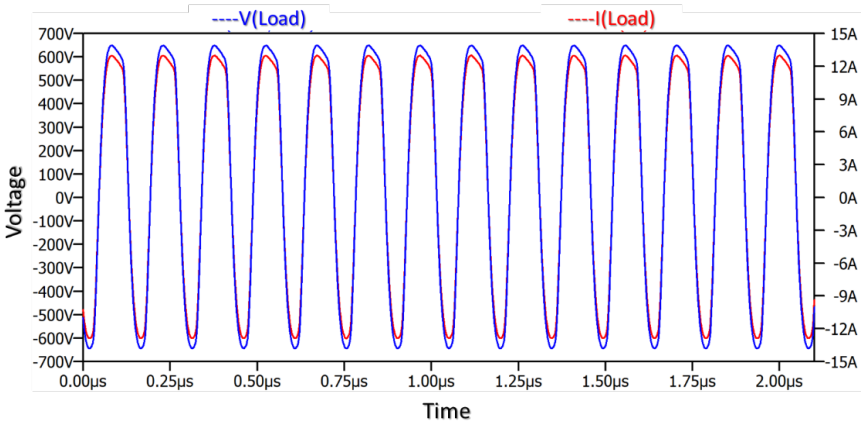

Fig. 8: Output load waveform of LC filter

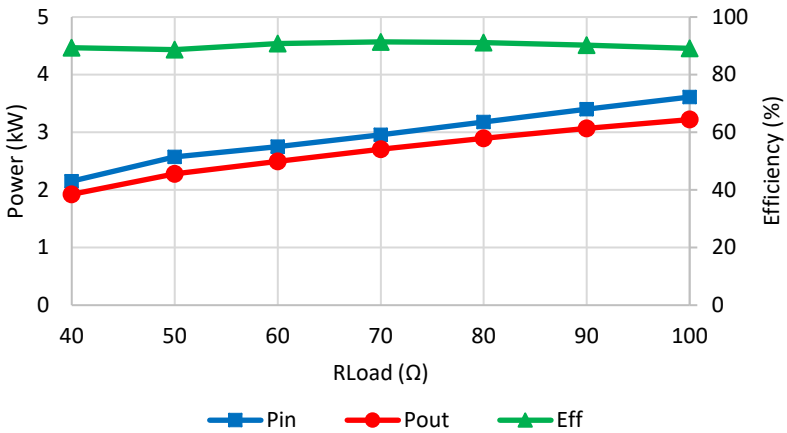

Fig. 9: Power and efficiency over load variation

Since a double voltage amplitude is achieved by the full bridge inverter, hence the peak-to-peak amplitude of the output signal from GaN MOSFET is illustrated in Fig. 7. It can be seen that the outputs of GaN MOSFETs 1 and 2 with GaN MOSFETs 3 and 4 are complementary or opposite, this shows that the calculation of dead time and GaN MOSFET conditions when ON and OFF is correct.

Pure sine wave signal is the goal to achieve in the full bridge inverter. By using the LC filter after the GaN MOSFET D1 and D2 pin, the output signal at the load side can be seen in Fig. 8. Because it has reached the complement between the outputs of the GaN MOSFET D1 and D2 then if the output is reduced to 1, the square signal when ON and OFF has shown values of 600 V and -600 V.

Based on the previous results, the full bridge inverter consisting of the designated value of all components then measured its efficiency. The measurement of power efficiency is done by calculating the consumed input power over the resulting output power under load variation from 10 to 100 Ω. Fig. 9 describes the measured input power; Pin, output power; Pout, and obtained power efficiency; Eff, over several load variations. It can be seen that the designated full bridge inverter can deliver 2 kW to 3.2 kW of power to the load and consumed power from 2.2 kW to 3.6 kW under load variation. For the 50 Ω load, it can have 89% power efficiency while transmitting 2.3 kW power to the load.

5. Conclusions

This paper has described the design a full bridge inverter based on GaN MOSFET for the capacitively WPT EV charging system by utilizing linear simulation software, here LTSpice. By performing calculations for the delay time, dead time, and also impedance matching components followed by the LC filter components, the simulation has analyzed and measured the consumed power, delivered power, and power efficiency. With an operating frequency of 13.56 MHz which is in line with the regulation from the ISM band, the inverter can deliver power from 2 kW to 3.2 kW with efficiency obtained from 89% to 91% under several load variations. With these results, it can be concluded that the full bridge inverter can produce a stable and efficient system in order to be implemented in the EV charging system. Future works related to the high-frequency inverter fabrication, impedance matching development, and integration of wireless charging experimental will proceed following the installation of the receiver part placed under the EV chassis.

Acknowledgements

The author would like to thank the Research Organization for Electronics and Informatics, National Research and Innovation Agency for supporting the funding for this research. All authors acknowledged the content of this manuscript.

References

1) T.M. Mostafa, A. Muharam, and R. Hattori, "Wireless battery charging system for drones via capacitive power transfer," in: 2017 IEEE PELS Workshop on Emerging Technologies: Wireless Power Transfer (WoW), IEEE, Chongqing, China, 2017: pp. 1–6. doi:10.1109/WoW.2017.7959357.
2) A. Muharam, T.M. Mostafa, A. Nugroho, A. Hapid, and R. Hattori, "A Single-Wire Method of Coupling Interface in Capacitive Power Transfer for Electric Vehicle Wireless Charging System," in: 2018 International Conference on Sustainable Energy Engineering and Application (ICSEEA), IEEE, Tangerang, Indonesia, 2018: pp. 39–43. doi:10.1109/ICSEEA.2018.8627079.
3) A. Muharam, T.M. Mostafa, and R. Hattori, "Design of power receiving side in wireless charging system for UAV application," in: 2017 International Conference on Sustainable Energy Engineering and Application (ICSEEA), IEEE, Jakarta, Indonesia, 2017: pp. 133–139. doi:10.1109/ICSEEA.2017.8267698.
4) L. Shi, P. Alou, J.A. Oliver, J.C. Rodriguez, A. Delgado, and J.A. Cobos, "A self-adaptive wireless power transfer system to cancel the reactance," *IEEE Transactions on Industrial Electronics*, **68** (*12*) 12141–12151 (2021). doi:10.1109/TIE.2020.3044817.
5) S.Y.R. Hui, W. Zhong, and C.K. Lee, "A critical review of recent progress in mid-range wireless power transfer," *IEEE Trans Power Electron*, **29** (*9*) 4500–4511 (2014). doi:10.1109/TPEL.2013.2249670.
6) K. Hashizaki, S. Dobashi, S. Okada, T. Hirai, J. Yamaki, and Z. Ogumi, "Charge-discharge characteristics of li/cucl_2 batteries with lipf_6/methyl difluoroacetate electrolyte," *Evergreen*, **6** (*1*) 1–8 (2019). doi:10.5109/2320995.
7) T. Tsubota, A. Kitajou, and S. Okada, "O3-type na(fe_1/3mn_1/3co_1/3)o_2 as a cathode material with high rate and good charge-discharge cycle performance for sodium-ion batteries," *Evergreen*, **6** (*4*) 275–279 (2019). doi:10.5109/2547348.
8) M. Nizam, Mufti Reza Aulia Putra, and Inayati, "Heat management on lifepo4 battery pack for eddy current brake energy storage on rapid braking processes," *Evergreen*, **9** (*2*) 451–456 (2022). doi:10.5109/4794171.
9) S. Sawant, R.M.R. Ahsan Shah, M. Rahman, A.R. Abd Aziz, S. Smith, and A. Jumahat, "System modelling of an electric two-wheeled vehicle for energy management optimization study," *Evergreen*, **8** (*3*) 642–650 (2021). doi:10.5109/4491656.
10) A. Yousefian, and N. Yamamoto, "3D finite difference time domain simulation of microwave propagation in a coaxial cable," *Evergreen*, **5** (*3*) 1–11 (2018). doi:10.5109/1957495.
11) A. Clements, V. Vishnoi, S. Dehghani, and T. Johnson, "A comparison of gan class e inverter and synchronous rectifier designs for 13.56 mhz, 27.12 mhz and 40.68 mhz ism bands," *2018 IEEE Wireless Power Transfer Conference, WPTC 2018*, 1–4 (2019). doi:10.1109/WPT.2018.8639292.
12) X. Wei, H. Sekiya, T. Nagashima, M.K. Kazimierczuk, and T. Suetsugu, "Steady-state analysis and design of class-d zvs inverter at any duty ratio," *IEEE Trans Power Electron*, **31** (*1*) 394–405 (2016). doi:10.1109/TPEL.2015.2400463.
13) H. Tebianian, Y. Salami, B. Jeyasurya, and J.E. Quaicoe, "A 13.56-mhz full-bridge class-d zvs inverter with dynamic dead-time control for wireless power transfer systems," *IEEE Transactions on Industrial Electronics*, **67** (*2*) 1487–1497 (2020). doi:10.1109/TIE.2018.2890505.
14) P. Jayathurathnage, M. Vilathgamuwa, and C. Simovski, "Revisiting Two-Port Network Analysis for Wireless Power Transfer (WPT) Systems," in: 2018 IEEE 4th Southern Power Electronics Conference (SPEC), IEEE, 2018: pp. 1–5. doi:10.1109/SPEC.2018.8635846.
15) M.A. de Rooij, "The ZVS voltage-mode class-D amplifier, an eGaN® FET-enabled topology for highly resonant wireless energy transfer," in: 2015 IEEE Applied Power Electronics Conference and Exposition (APEC), IEEE, 2015: pp. 1608–1613. doi:10.1109/APEC.2015.7104562.
16) C.T. Rim, and C. Mi, "Wireless Power Transfer for Electric Vehicles and Mobile Devices," John Wiley & Sons, 2017.
17) C. Lecluyse, B. Minnaert, and M. Kleemann, "A review of the current state of technology of capacitive wireless power transfer," *Energies (Basel)*, **14** (*18*) 5862 (2021). doi:10.3390/en14185862.
18) M. Kline, I. Izyumin, B. Boser, and S. Sanders, "Capacitive power transfer for contactless charging," in: 2011 Twenty-Sixth Annual IEEE Applied Power Electronics Conference and Exposition (APEC), IEEE, 2011: pp. 1398–1404. doi:10.1109/APEC.2011.5744775.
19) Innovation Science and Economic Development Canada, "Spectrum Management and Telecommunications Interference-Causing Equipment Standard Industrial, Scientific and Medical (ISM) Equipment," 2020.
20) A. Muharam, T.M. Mostafa, S. Ahmad, M. Masuda, D. Obara, R. Hattori, and A. Hapid, "Preliminary

study of 50 w class-e gan fet amplifier for 6.78 mhz capacitive wireless power transfer," *Journal of Mechatronics, Electrical Power, and Vehicular Technology*, **11** (*1*) 22–29 (2020). doi:10.14203/j.mev.2020.v11.22-29.

21) P. Sharma, J. Pande, and A. Singh, "Comparative implication and analysis of inductive & capacitive wireless power and data transfer in usb," *International Journal of Innovative Research in Advanced Engineering (IJIRAE)*, **2** (*1*) 247–253 (2015).
22) A.I. Mashhadi, B. Poorali, S. Hor, M. Pahlevani, and H. Pahlevani, "A new wireless power and data transmission circuit for cochlear implants," *Wireless Power Week*, 1–4 (2019).
23) X. Li, J. Hu, H. Wang, X. Dai, and Y. Sun, "A new coupling structure and position detection method for segmented control dynamic wireless power transfer systems," *IEEE Trans Power Electron*, **35** (*7*) 6741–6745 (2020). doi:10.1109/TPEL.2019.2963438.
24) R. Erfani, F. Marefat, A.M. Sodagar, and P. Mohseni, "Modeling and experimental validation of a capacitive link for wireless power transfer to biomedical implants," *IEEE Transactions on Circuits and Systems II: Express Briefs*, **65** (*7*) 923–927 (2018). doi:10.1109/TCSII.2017.2737140.
25) Z. Wang, Y. Zhang, X. He, B. Luo, and R. Mai, "Research and application of capacitive power transfer system: a review," *Electronics (Basel)*, **11** (*7*) 1158 (2022). doi:10.3390/electronics11071158.
26) J. Xu, L. Gu, Z. Ye, S. Kargarrazi, and J. Rivas-Davila, "Cascode gan/sic power device for mhz switching," *Conference Proceedings - IEEE Applied Power Electronics Conference and Exposition - APEC*, **2019-March** 2780–2785 (2019). doi:10.1109/APEC.2019.8721931.